Chapter 2
Stationary Creep

Abstract An introduction to creep and its main characterstics are given. Stationary creep has been studied extensively in the literature. Stationary creep is a result of a balance between work hardening and recovery processes, which allows for a continues plastic deformation without raising the stress. The starting point for the basic modeling of creep is a differential equation for the dislocation density that describes how it varies with strain or time. The model explains how the dislocation density is influenced by work hardening and recovery. From the dislocation model, a basic equation for the creep rate is derived that is in many respects similar to the classical Bird, Mukherjee and Dorn (BMD) formula but with the values of the parameters given. By taking the role of strain induced vacancies into account, the applicability of the BMD equation is widely expanded because the basic model can also handle low temperatures and high stresses that is usually referred to as the power-law break down regime. It is illustrated that the creep model can represent the creep rate for pure metals such as Al and Ni.

2.1 The Creep Process

Creep deformation is in general assumed to take place by the motion of dislocations. At very low stress and high temperatures creep can also occur by the diffusion of individual atoms, which is referred to as diffusion creep. The framework for diffusion creep and the competing dislocation creep at very low stresses are discussed in Chap. 5. In this chapter the focus will be on dislocation creep.

Let us consider a specimen in a soft annealed condition. During a creep test the few dislocations present initially will rapidly multiply and form a network. This network will strengthen the material, which is referred to as *work hardening*. In a polycrystalline metal, the initial phase of the work hardening is characterized by an increase in the strength from the dislocations that is proportional to the strain. Gradually the dislocation density becomes sufficiently high that more stable and energy efficient dislocation structures are formed that reduce the increase in strength. During this stage also some dislocations are eliminated due to the interaction with

R. Sandström, *Basic Modeling and Theory of Creep of Metallic Materials*, Springer Series in Materials Science 339,
https://doi.org/10.1007/978-3-031-49507-6_2

other dislocations. Thus there is a process that balances the work hardening and removes and stabilizes some dislocations. We will refer to this process as *dynamic recovery*. It is strain controlled in the same way as the work hardening. The stages described so far are similar for creep and rate controlled tensile tests.

Specific for creep is that there is an additional process called *static recovery*. Dislocations with opposite burgers vectors attract each other and if the dislocations are free to move, they will eventually eliminate each other. At low temperatures dislocations can only move in their glide planes, which is referred to as glide. At high temperatures the dislocations can also move perpendicular to the glide planes. For edge dislocations this is possible if atoms can diffuse to and from the dislocation cores. This mechanism is called climb. The main difference between plastic deformation at low and at high temperatures is that climb of dislocations can take place. This enables that dislocations can move both parallel and perpendicular to the glide planes. This is crucial during static recovery since the dislocations that are influenced by attracting forces can reach each other. This makes it possible for dislocations to annihilate each other and that is the basis of static recovery.

When the dislocation density has reached a certain level during a creep test due to work hardening, the static recovery starts to be of importance. There is work hardening that raises the dislocation density and recovery that reduce the density. The rates of recovery increase faster with time than the rate of work hardening. This means that eventually there will be a balance between work hardening and recovery. The whole process becomes stationary and the dislocation density becomes constant. This is referred to as stationary creep. In the traditional way of describing a creep strain versus time curve ("creep curve"), stationary creep is the second stage and therefore it is referred to as secondary creep as well. Although stationary and secondary creep does not always be exactly the same thing, no distinction between the terms will be made in the present book.

The presence of a stationary stage implies that a specimen can continue to deform at constant stress or load, which is one of the most characteristic features of creep, and any basic creep model must be able to describe how the stationary stage is reached. In creep strain tests, the secondary creep rate is usually measured as the minimum creep rate. Even in the secondary stage, the creep rate is not fully constant. The extent of the secondary stage is rarely precisely defined and it is up to the one analyzing the creep data to determine that.

Two types of recovery, dynamic and static, are introduced above. In fact, in most papers where recovery during creep is discussed no distinction is made between dynamic and static recovery. In addition, the nomenclature varies. In this book dynamic recovery is strain controlled and static recovery time controlled. This means that dynamic recovery only takes place when a specimen is strained whereas static recovery can occur even without external load. To describe both tensile and creep tests with the same models, both dynamic and static recovery must be taken into account. In addition, there are a number of phenomena such as the role of cell structure and the influence of cold work on creep that would be very difficult to describe without taking both types of recovery into account.

In Sect. 2.2 empirical models for the secondary creep rate are presented. The dislocation model that is the basis for the description of both stress controlled (creep) and rate controlled (stress strain curves) deformation is derived in Sect. 2.3. Some constants that are needed in the creep models are analyzed in Sect. 2.4. The basic formula for the secondary creep rate is given in Sect. 2.5. The dislocation mobility plays a central role in the modeling, Sect. 2.6. Finally in Sect. 2.7, the analysis is applied to aluminum and in Sect. 2.8 to nickel.

2.2 Empirical Models of Secondary Creep

It was early on recognized that the creep rate in the secondary stage could be described with simple relations. Norton found that stress dependence of the creep rate $\dot{\varepsilon}_{\text{sec}}$ could be described with an exponential expression [1]

$$\dot{\varepsilon}_{\text{sec}} = A_{\text{N}}\sigma^{n_{\text{N}}} \tag{2.1}$$

where σ is the applied stress A_{N} is a constant. n_{N} is referred to as the stress or Norton exponent. Equation (2.1) was later extended by including the temperature and grain size dependence [2, 3]

$$\dot{\varepsilon}_{\text{sec}} = \frac{A_{\text{N}} D_{\text{self}} G b}{k_{\text{B}} T}\left(\frac{b}{d}\right)^{p}\left(\frac{\sigma}{G}\right)^{n_{\text{N}}} \tag{2.2}$$

D_{self} is assumed to be the self-diffusion coefficient represented with an Arrhenius expression $D_{\text{s0}} \exp\left(-Q_{\text{self}}/R_{\text{G}}T\right)$ where D_{s0} is a frequency factor, Q_{self} an activation energy, and R_{G} the gas constant. G is the shear modulus, b the Burgers vector, k_{B} the Boltzmann's constant, T the absolute temperature, d the grain size, σ the applied stress, and A_N a constant. The constant p is the grain size exponent that is usually close to zero but takes positive values for fine grained materials. A_{N}, p and n_{N} are usually considered as adjustable parameters and fitted to experimental data. Unless the activation energy is close to that for self-diffusion, it is an additional adjustable parameter. Equation (2.2) is often referred to as the Bird, Mukherjee and Dorn (BMD) equation. The equation has been much used in creep research in the past decades. It has been assumed that from the values of the stress exponent, the activation energy and the grain size exponent, the active mechanisms could be identified. This will first be analyzed for the stress exponent below.

Another reason for the importance of Eq. (2.2) is that the creep rate can roughly be related to the rupture time with the help of the Monkman-Grant relationship [4]

$$\dot{\varepsilon}_{\text{sec}}^{m_{MG}} t_R = C_{MG} \tag{2.3}$$

where t_{R} is the time to rupture and m_{MG} and C_{MG} are constants. The relation works

best when the secondary stage is a fairly large fraction of the creep life. An alternative way of writing Eq. (2.3) is

$$\dot{\varepsilon}_{\text{sec}} t_R = \varepsilon_{R_{\text{sec}}} \tag{2.4}$$

where $\varepsilon_{R\text{sec}}$ is the total creep strain in the secondary stage. Equation (2.4) is often easier to apply than (2.3).

The understanding of dislocation creep is mainly based on modeling. The prime interest has been on secondary creep. The reason is that the stress dependence of the rate in the secondary stage has been assumed to reflect the operating creep mechanism. In two papers Weertman suggested that stress exponent was about 5 if climb of dislocations and about 3 if glide of dislocations was controlling [5, 6]. This resulted in the anticipation that the value of the stress exponent could be used to identify the controlling microstructure mechanism. This was further emphasized by the predictions of the diffusion creep models that gave a stress exponent of 1.

Creep investigations concerning metals have often been performed above half the absolute melting point T_{m}. In Fig. 2.1, the stress dependence of the creep rate is illustrated for 0.5Cr0.5Mo0.25V steel at 565 °C over a wide range of stresses.

The slope of the curve gives the stress exponent n_{N}. At intermediate stresses (and temperatures) the stress exponent is usually in the range 3–8. The value in Fig. 2.1 is 4. The stress exponent is much higher at high stresses (and at low temperatures), in the Figure illustrated with $n_{\text{N}} = 12$. The creep rate varies exponentially with stress at still higher stresses, which is referred to as power-law breakdown. This can give very high stress exponents. At very low stresses, the n_{N} value takes values down to unity or even below unity [7]. The steel 0.5Cr0.5Mo0.25V is a precipitation hardened material. Other precipitation hardened alloys can show much higher stress exponents than in Fig. 2.1.

Climb of dislocations has in general been considered as the operating mechanism at intermediate exponents (3–8). However, glide has also been proposed to control the

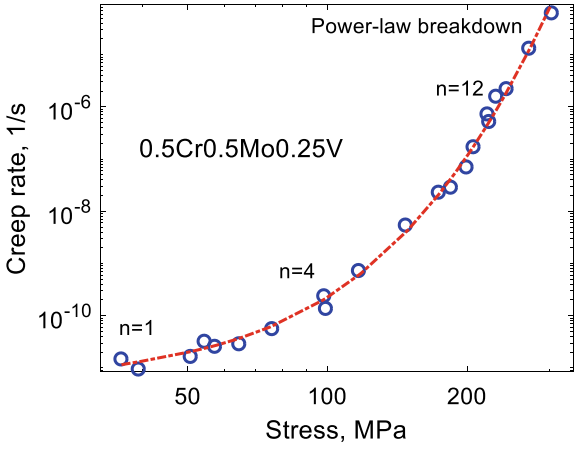

Fig. 2.1 Creep rate versus stress for 0.5Cr0.5Mo0.25V steel at 565 °C. The *n* value is the stress exponent in the power-law creep law, Eq. (2.2). At large stresses the creep rate increases exponentially with the stress, which is called power-law breakdown. Some of the data points are extrapolated. After Wilshire [7]. Reprinted from [8] with permission of intechopen

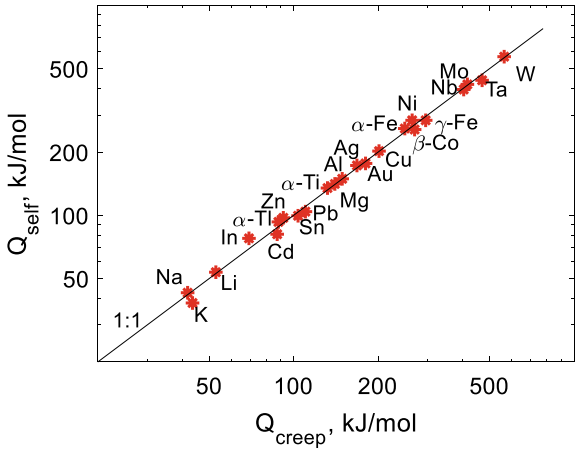

Fig. 2.2 Activation energy for self-diffusion Q_{self} versus the activation energy for creep Q_{creep}. Q_{creep} is obtained by fitting the Q value in Eq. (2.2) to creep strain rate data. After Sherby and Miller [3]

deformation for certain alloy types. The dominating mechanism at high stresses has been suggested as glide. The main mechanism at low stress exponents approaching 1 has been considered to be diffusion creep. This consistent change of operating mechanism with stress has been challenged, see for example [7]. Recent research supports that this challenge is relevant. This will be discussed in Sect. 2.6.4.

It was early on recognized that when the activation energy in Eq. (2.2) was fitted to creep strain data for pure metals a value close to the activation energy for self-diffusion Q_{self} was obtained. This was the reason for having the self-diffusion coefficient in Eq. (2.2). The fitted value is referred to as the activation energy for creep Q_{creep}. The relation between Q_{creep} and Q_{self} is illustrated in a classical picture in Fig. 2.2 [2, 3].

The natural explanation of the close relation between Q_{creep} and Q_{self} is that creep is controlled by climb. Since climb requires the diffusion of vacancies, the climb rate of pure metals is proportional to the constant for self-diffusion. However, for alloyed steels the activation energy for creep can be significantly higher than for self-diffusion due to solid solution hardening. There are other mechanisms that give a creep rate that is related to the self-diffusion constant. The most well-known one is diffusion creep.

2.3 Dislocation Model

The most characteristic feature of creep is that there is a continuous deformation at constant load or stress. This requires that extensive recovery of dislocations takes place that balances the strengthening effect of dislocations due to work hardening. Basic creep models must be able to describe this feature. This is the basis of creep recovery theories [9]. To provide creep models that can make general predictions, the models must be based on basic physical principles and the use of adjustable

parameters must be avoided. In this chapter such a creep recovery model will be presented.

To describe plastic deformation, the development of the dislocation structure must be known. Only recently quantitative basic models have been established that fulfill the requirements in the previous paragraph. Such a model will now be presented. In later sections and chapters it will be used in a number of applications.

During plastic deformation three main processes take place. Work hardening raises the strength by generation of new dislocations and thereby increases their density. The increase of the dislocation density raises the energy content of the material. There is a driving force to reduce the energy content. The mechanism that makes this possible is called recovery. During recovery dislocations of opposite signs combine to form low energy configuration or annihilate each other, which reduces the density of dislocations. There are two types of recovery: dynamic recovery that is strain dependent and static recovery that is time dependent.

2.3.1 Work Hardening

The work hardening of polycrystalline materials can be described with the help of the following equation for the dislocation density ρ

$$\frac{d\rho}{d\varepsilon} = \frac{m_\mathrm{T}}{bL_\mathrm{s}} \qquad \text{(work hardening)} \tag{2.5}$$

ε is the strain, m_T the Taylor factor, b Burger's vector and L_s the "spurt" distance which the dislocation moves in each elementary release during deformation for example from a Frank-Read source. Equation (2.5) can be derived from the Orowan equation

$$\dot{\varepsilon} = b\rho v/m_\mathrm{T} \tag{2.6}$$

$\dot{\varepsilon}$ is the creep rate and v the velocity of the dislocations. If Eq. (2.6) is integrated, one obtains

$$\varepsilon = b\rho L_\mathrm{s}/m_\mathrm{T} \tag{2.7}$$

This equation describes how much strain is generated when the dislocations have spurted a distance L_s. If we derivate Eq. (2.7) and keep the spurt distance L_s constant, we get Eq. (2.5). The Orowan Eq. (2.6) is based only on a geometrical argument and not on a specific mechanism, and this applies to Eqs. (2.5) and (2.7) as well. In this way these equations have a general applicability. In Eq. (2.5), L_s can be related to the barriers in the materials such as grains or subboundaries. The simplest assumption is that the spurting dislocations are stopped by the grain boundaries. L_s would then be the grain size d_g. This would give a grain size dependence in the creep rate that

is not observed except in special cases. The most common assumption is that L_s is controlled by the forest of dislocations, i.e. it is related to the average distance between the dislocations $1/\rho^{1/2}$.

$$L_s = \frac{c_L}{\rho^{1/2}} \tag{2.8}$$

c_L is a constant that is much larger than unity. How to find the size of c_L will be discussed below. If the dislocations are stopped by the subboundaries instead it gives an L_s value that is not very different from that in Eq. (2.8) as will be seen below. If Eq. (2.8) is inserted into Eq. (2.5) one finds that

$$\frac{d\rho}{d\varepsilon} = \frac{m_T \rho^{1/2}}{b c_L} \qquad \text{(work hardening)} \tag{2.9}$$

This form of the work hardening equation appears in many models including empirical ones, see for example [10, 11]. As will be seen below, this model can describe the initial stages of work hardening in fcc alloys.

2.3.2 Dynamic Recovery

When two dislocations during plastic deformation are nearer to each other than a critical distance d_{int} a low energy configuration may be formed or annihilation occurs reducing the dislocation density. This process is referred to as dynamic recovery. It is commonly taken into account with the help of the following equation

$$\frac{d\rho}{d\varepsilon} = -\omega\rho \tag{2.10}$$

where ω is a constant. This equation was first proposed by Bergstrom and co-workers [12, 13]. Roters et al. [14] gave a basic derivation of Eq. (2.10). They used the following argument. During a time increment dt a dislocation travels a distance v dt and has to find a suitable dislocation within the distance $2d_{int}$. This gives an annihilation rate of

$$d\rho = -\rho v dt 2d_{int}\rho = -\frac{\dot{\varepsilon} m_T}{b} dt 2d_{int}\rho \tag{2.11}$$

In the last step, the Orowan Eq. (2.6) has been applied. This gives an equation of the same form as Eq. (2.10). By taking the role of slip planes, dislocation locks and dislocation dipoles into account, the following expression for the constant ω was obtained [14]

$$\omega = \frac{m_T}{b} d_{int} \left(2 - \frac{1}{n_{slip}} \right) \tag{2.12}$$

n_{slip} is the number of independent slip systems (=12 for fcc metals). Roters et al. [14] suggested a high value for d_{int}. But in fact d_{int} is quite small [15]. The simplest way to estimate d_{int} is to assume that it is equal to twice the dislocation core radius. For example, ab initio calculations for copper give a core radius of $r_0 = 1.3\ b$ [16], and thus $d_{int} = 2.6\ b$. This gives $\omega = 15$ which is quite a good value for copper in agreement with observations. To represent dynamic recovery, Eq. (2.10) is a common equation to use. Together with Eq. (2.9), work hardening of many materials can be described [10, 11]. Equation (2.10) has been used in many papers for representing stress strain curves. A list of such papers can be found in [17].

2.3.3 Static Recovery

Dislocations of opposite burgers vector attract each other. Static recovery takes into account how climbing (and gliding, see below) dislocations of opposite signs move towards each other and finally annihilate. This can be described by the following equation

$$\frac{d\rho}{dt} = -2\tau_L M \rho^2 \tag{2.13}$$

t is the time, τ_L the dislocation line tension, and M the dislocation climb mobility. The idea behind this equation was suggested by Friedel [18], but he never gave any derivation of it in his book. The equation was first used extensively by Lagneborg and co-workers [9]. To derive the equation, let us consider a network of dislocations with an average spacing of R, which corresponds to a dislocation density of $\rho = 1/R^2$. With the help of the dislocation mobility, the velocity of the dislocations can be estimated

$$\frac{dR}{dt} = -Mb\sigma = -Mb\frac{Gb}{2\pi R} \ln\left(\frac{R}{r_0}\right) = -\frac{M\tau_L}{R} \tag{2.14}$$

G is the shear modulus. In the second equality, the expression for the stress from a neighboring screw dislocation is introduced. In the third equality, an expression for the line tension of a screw dislocation has been applied. If equations for edge dislocations or mixed screw and edge dislocations are used instead, the end result is the same. The time to eliminate the dislocation pair t_{elim} is obtained by integrating Eq. (2.14) with respect to time

$$t_{elim} = \frac{R^2}{2M\tau_L} \tag{2.15}$$

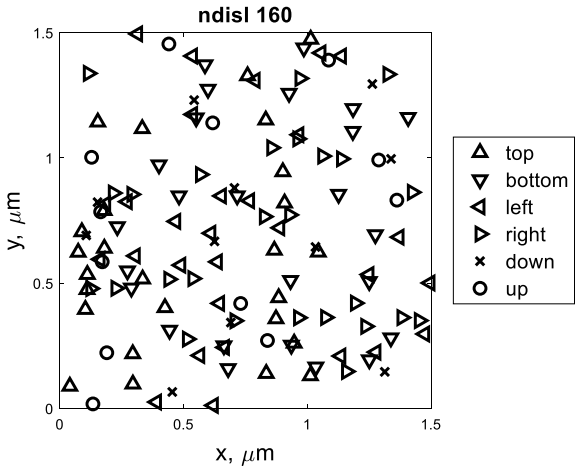

Fig. 2.3 Dislocation dynamics simulation in 2D of static recovery. There are edge dislocations with four Burgers vectors (in the directions top, bottom, left, right) and screw dislocations with two Burgers vectors (in the directions down, up). 160 dislocations remain in the simulation

The average distance between the dislocations changing with time during the recovery is obtained from Eq. (2.15)

$$\frac{dR}{dt} = \frac{M\tau_{\mathrm{L}}}{R} \tag{2.16}$$

If now the relation $R = 1/\sqrt{\rho}$ is applied to Eq. (2.16), (2.13) is recovered.

The derivation of the rate for static recovery, Eq. (2.13), is obviously simplified since it considers only a pair of dislocations. To analyze static recovery in a more general situation, dislocation dynamic simulations have been performed. Randomly distributed parallel dislocations with six different Burgers vectors have been studied, see Fig. 2.3. Four of the sets were edge dislocations and two screw dislocations. Dislocations of opposite signs attract each other (top, bottom or left, right or down, up) and eventually annihilate.

The result of the analysis is illustrated in Fig. 2.4. In this case 1300 dislocations were used in the simulation. In Fig. 2.4 the values from Eq. (2.13) are scaled to the same number of initial dislocations.

It is evident from Fig. 2.4 that the validity of Eq. (2.13) is not restricted to a single pair of dislocations.

Equation (2.13) is based on the annihilation of forest dislocations, i.e. dislocations in the subgrain interiors. If the static recovery is based on subgrain coarsening instead, the recovery rate can be derived with the help of the results in [19]. In fact, the same results as before are obtained, i.e. Eq. (2.13) is reproduced. Thus, the role of the subgrains cannot be determined from the form of Eq. (2.13). Blum has suggested that taking substructure into account would change the recovery process [20]. This obviously depends on the details of the assumptions.

Both dynamic and static recovery are based on the annihilation of dislocations of opposite Burgers' vector or orientation that come close to each other. Although the

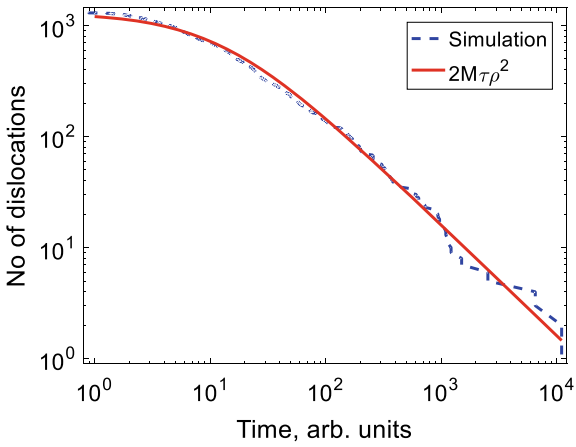

Fig. 2.4 Number of dislocations versus time during static recovery. Dislocation simulation results are compared with Eq. (2.13)

modelling of dynamic and static recovery are strain and time controlled, respectively, and they are based on the different derivations, the two recovery mechanisms are not completely unrelated. For some processes, it is essential to take both types of recovery into account, for example, for stress strain curves for large strains and for primary creep. For more limited strain ranges, dynamic recovery is enough to consider for stress strain curves. On the other hand, the stationary creep rate is based on static recovery. In some cases, it is even assumed that the two recovery mechanisms can give the same results. This is the case in one derivation of the c_L parameter. Dynamic and static recovery should be considered as different appearances of the same phenomenon, and their relative importance depends on the application. Their final role should always be verified by comparison to experiments. The varying influence of the two types of recovery could be compared with phenomena in quantum mechanics, which could be explained in terms of particles or wave packages or both.

2.3.4 Accumulated Dislocation Model

To describe how the dislocation density ρ develops during plastic deformation, the contributions from work hardening (2.5), dynamic recovery (2.10), and static recovery (2.13) are added.

$$\frac{d\rho}{d\varepsilon} = \frac{m_T}{bc_L}\rho^{1/2} - \omega\rho - 2\tau_L M\rho^2/\dot{\varepsilon} \tag{2.17}$$

Notice that we have strain derivatives in (2.5) and (2.10) but a time derivative in (2.13). By multiplying or dividing by $\dot{\varepsilon}$, one can make a transformation from one type of derivative to the other. Equation (2.17) represents a general basic equation

for the development of the dislocation density during plastic deformation. We have seen above that all parts of Eq. (2.17) have a good basis.

The validity of the two first two terms on the right hand side (RHS) of Eq. (2.17) has been verified by comparison to the work hardening in tensile tests. This will be further discussed in Chap. 3. The experimental verification of the last term, the static recovery term is done with the help of creep tests. Examples will be given below.

In many papers in the literature either dynamic or static recovery is taken into account but not both. However, there are cases where it is absolutely essential to include both. For example, this is the case for the influence of cold working on creep properties, which will be treated in Sect. 8.3 [21]. In addition, if the same equation is to be used to describe both strain rate and stress controlled tests, both dynamic and static recovery must be included. Equation (2.17) has to be expanded for some types of materials. A well-known case is martensitic 9 and 12% Cr-steels. For example, to describe primary creep more than one type of dislocation density must be taken into account [22]. This will be described in Sect. 4.5.

2.4 The c_L Parameter

The value of the c_L parameter can be found from the following analysis. The maximum dislocation density ρ_x that is derived from Eq. (2.17) plays an important role because it gives the dislocation contribution to the creep strength during stationary conditions and the amount of work hardening during tensile tests.

The main alternative to derive the value of c_L. is to make reference to the substructure. The spurt distance L_s in Eq. (2.5) can be related to the subgrain or cell diameter d_{sub}.

$$L_s = n_{sub} d_{sub} \tag{2.18}$$

where the constant n_{sub} is close to 3 [23, 24]. It is well established that the subgrain or cell size can be related to the dislocation stress

$$d_{sub} = \frac{K_{sub} G b}{\sigma_{disl}} \tag{2.19}$$

K_{sub} is a constant typically in the range 10–20 [25]. The dislocation stress σ_{disl} is given by Taylor's equation

$$\sigma_{disl} = \alpha m_T G b \rho^{1/2} \tag{2.20}$$

where σ_{disl} is the strength contributions from the dislocations. This equation gives the relation between the strength contribution from the dislocations and the dislocation density where $\alpha \approx 0.19$ is a constant. Experimentally α takes typically values in

the range 0.2–0.6 [26]. In this book a computed value $\alpha \approx 0.19$ applicable to high temperatures will be used, Eq. (3.17). Equation (2.18) can now be rewritten as

$$L_s = \frac{n_{sub} K_{sub} G b}{\sigma_{disl}} = \frac{n_{sub} K_{sub}}{m_T \alpha \rho^{1/2}} \tag{2.21}$$

Equation (2.21) has the same form as Eq. (2.8) so a c_L value can be obtained directly

$$c_L = \frac{n_{sub} K_{sub}}{m_T \alpha} \tag{2.22}$$

A simple estimate of the c_L value can be obtained in the following way. It is assumed that the maximum dislocation density ρ_x is either controlled by the dynamic recovery term (ρ_{xdr}) or the static recovery term (ρ_{xsr}) in Eq. (2.17)

$$\rho_{xdr} = \left(\frac{m_T}{b c_L \omega}\right)^2 \qquad \rho_{xsr} = \left(\frac{m_T \dot{\varepsilon}}{2 b c_L \tau_L M}\right)^{2/3} \tag{2.23}$$

At ambient temperatures, the stress dependence of the recovery terms is such that the dynamic recovery term dominates. This means that first of Eq. (2.23) is the one that is applicable and can be used to obtain an estimate of c_L.

$$c_L = \frac{m_T}{b \omega \rho_x^{1/2}} = \frac{m_T^2 \alpha G}{\omega \sigma_{dislx}} \approx \frac{m_T^2 \alpha G}{\omega (R_m - \sigma_y)} \tag{2.24}$$

where R_m is the tensile strength and σ_y the yield strength at room temperature. In the second equality, Taylor's Eq. (2.20) has been applied. In the final equality in Eq. (2.24), the maximum value of σ_{disl} has been estimated as the difference between the tensile strength R_m and the yield strength σ_y for a material without significant contributions from precipitation and solid solution hardening. The ratio between the expressions for static and dynamic recovery, Eqs. (2.13) and (2.10), is given by

$$\frac{2 \tau_L M \rho}{\omega \dot{\varepsilon}}$$

Apart from constants this is the same ratio as in the creep Eq. (2.28), see below, if the ratio is multiplied by $\rho^{1/2}$. This means that the following ratio is at least approximately temperature and stress independent

$$\frac{2 \tau_L M}{\omega \dot{\varepsilon}} \rho^{3/2}$$

To make Eq. (2.24) valid at higher temperature, we have to multiply it by $(\rho(T)/\rho(T_{RT}))^{1/2}$ which gives

$$c_{\mathrm{L}} = \frac{m_{\mathrm{T}}}{b\omega\rho(T)^{1/2}}\left(\frac{\rho(T)}{\rho(T_{\mathrm{RT}})}\right)^{1/2} = \frac{m_{\mathrm{T}}}{b\omega\rho(T_{\mathrm{RT}})^{1/2}} \tag{2.25}$$

where T_{RT} is the room temperature. This expression is identical to Eq. (2.24). This means that Eq. (2.24) is valid at elevated temperatures as well. Consequently, c_{L} is a temperature independent constant. Eq. (2.22) represents a more physically based value than Eq. (2.24), but the values are of the same order.

Another argument can in a number of cases give a more accurate estimate of c_{L}. It is well-known that tensile stress strain tests can give rise to a stationary stress level if sufficiently large strains can be reached. This stress level is comparable to the creep stress that gives the same strain rate that was used in the tensile test. For many creep tests the contribution from the static recovery is dominating that of dynamic recovery. On the other hand for stress strain curves, the situation is reversed: dynamic recovery is more important than static recovery. But the comparison between the results from the tensile and the creep tests gave the same stationary results. A possible assumption is then that dynamic recovery and static recovery should generate the same findings. Putting it in mathematical terms this means that the two last terms in Eq. (2.17) should be the same, which gives

$$\omega\dot{\varepsilon} - 2\tau_{\mathrm{L}}\rho_{\mathrm{s}}M_{\mathrm{cl}}(\rho_{\mathrm{s}}) \tag{2.26}$$

Since the climb mobility M_{cl} in general depends on the dislocation density, Eq. (2.26) has to be solved by iteration to find the stationary dislocation density ρ_{s}. This argument is only valid if only one of the dynamic or the static recovery term is taken into account. If the dynamic recovery term is considered, the first two terms on the RHS of Eq. (2.17) have the same value under stationary conditions and the c_{L} value can be determined.

$$c_{L=}\frac{m_{\mathrm{T}}}{b\omega}\rho_{\mathrm{s}}^{1/2} \tag{2.27}$$

This relation will be used in Sect. 3.3 for stress strain curves.

2.5 Secondary Creep Rate

The recovery theory is the basis of our understanding of the creep process [9]. For secondary creep to take place the recovery rate must be sufficiently fast that the dislocation density can be kept constant. In the presence of a continuously rising dislocation density, the creep rate will gradually be reduced and eventually vanish, which is not in accordance with observations. Thus, the balance between the generation and the annihilation of dislocations is a crucial feature. The strain derivative in Eq. (2.17) vanishes if we assume stationary conditions. The secondary strain rate can then be expressed as

$$\dot{\varepsilon}_{\text{sec}} = \frac{2\tau_{\text{L}} b c_{\text{L}}}{m_{\text{T}}} M_{\text{climb}} \rho^{3/2} \tag{2.28}$$

In Eq. (2.28) only static recovery is taken into account, not dynamic recovery to make the equation agree with observations. This was discussed at the end of Sect. 2.3.3.

If other contributions than the dislocation stress is part of the applied stress, Eq. (2.20) has to be rewritten as

$$\sigma_{\text{disl}} = \alpha m_{\text{T}} G b \rho^{1/2} = \sigma - \sigma_i \tag{2.29}$$

σ_{disl} is the dislocation stress. σ_{i} is an internal stress that was the yield strength above. In addition, contributions from solid solution hardening and particle hardening can be included. They will be discussed in Chaps. 6 and 7. Equation (2.28) can be transformed to stresses with the aid of Taylor's Eq. (2.29),

$$\dot{\varepsilon}_{\text{sec}} = h_{\text{sec}}(\sigma - \sigma_i) \text{ where } h_{\text{sec}}(\sigma) = \frac{2\tau_{\text{L}} b c_{\text{L}}}{m_{\text{T}}} M_{\text{climb}}(T, \sigma) \frac{\sigma^3}{(\alpha m_{\text{T}} G b)^3} \tag{2.30}$$

The mobility M will be given below. At low stresses this expression is almost independent of stress, and Eq. (2.28) approximately gives a power-law expression with a stress exponent of 3 if there is no internal stress. This is sometimes referred to as the natural creep law [27]. This stress exponent is often observed at high temperatures for austenitic stainless steels [28]. There are many factors that influence the value of the stress exponent n_{N}. If diffusion takes place along dislocations (pipe diffusion) instead of in the grains, the stress exponent is increased by 2 [29]. If the dislocation network consists of dipoles instead of single dislocations the stress exponent is raised by 2, but limited experiments are available to support that [20]. But the most dramatic effect is from strain induced vacancies that will be analyzed in detail below.

According to Eq. (2.29), the applied stress σ is equal to the sum of the strength contributions from dislocations σ_{disl} and from other parts σ_{i} (solid solution and particle hardening). At low temperatures σ_{i} can also include the yield strength. Thus, for a pure metal the applied stress is equal to the dislocation strength if the yield strength is not taken into account. There are other formulations of the creep-recovery theory that also involve an effective stress σ_{eff}, see for example [30]. This means that Eq. (2.29) is replaced by

$$\sigma = \sigma_{\text{eff}} + \sigma_{\text{disl}} - \sigma_i \tag{2.31}$$

Physical arguments have been given for the existence of an effective stress [31]. However, the effective stress is a problematic quantity. It has been suggested that σ_{eff} could be measured in stress drop tests. If the dislocation structure is intact after a stress drop, the strain rate would disappear after a sufficiently large stress drop, because the back stress from dislocations would be much larger than for the stationary

level at the new lower stress. However, it is known now from dislocation dynamics simulations (DDS) that the forest dislocations adapt to the new stress level within milliseconds [32]. The substructure is also likely to partially adapt to the new stress level but not completely. So the back stress that is measured is from the unchanged part of the substructure. Unfortunately, no detailed studies on the momentary effect on the substructure seem to exist. It is evident that what is measured in a stress drop test is something that is quite different from what is supposed to be the effective stress. Stress drop tests at different laboratories have not in general given consistent results [33]. This is not surprising considering the dynamic nature of stress drop tests, which makes them very sensitive to the exact experimental setup [34]. In the present text, the effective stress will not be considered, since there seems to be no well-defined way to measure or model the quantity.

$$\sigma_{\text{eff}} = 0 \tag{2.32}$$

From the results that are presented in this text it will be evident that precise creep models can be formulated without introducing an effective stress.

2.6 Dislocation Mobility

2.6.1 Climb Mobility

The dislocation mobility M in Eq. (2.17) describes the velocity v of moving dislocations

$$v = Mb\sigma \tag{2.33}$$

where σ is the applied stress. Glide of dislocations takes place in their slip planes and climb perpendicular to the slip planes. Climb is associated with the emission and absorption of vacancies by diffusion. Climb is a slower process than glide. Hirth and Lothe [35] derived a basic expression for the climb mobility of pure metals at high temperatures (>0.4 T_{m} where T_{m} is the melting temperature)

$$M_{\text{climb0}} = \frac{D_{\text{s0}} b}{k_{\text{B}} T} e^{\frac{\sigma b^3}{k_{\text{B}} T}} e^{-\frac{Q_{\text{self}}}{R_{\text{G}} T}} \tag{2.34}$$

where T is the absolute temperature, σ the applied stress, D_{s0} the pre-exponential coefficient for self-diffusion, Q_{self} the activation energy for self-diffusion, k_{B} Boltzmann's constant, and R_{G} the gas constant.

At lower temperatures, plastic deformation raises the number of vacancies above the equilibrium value. A climbing dislocation will either emit or absorb vacancies. Jogs in the form of steps of the length of a Burgers vector are formed on gliding

dislocations when they cut each other. In general jogs move by climb and hence they also emit or absorb vacancies. Since the climb rate is proportional to the number of vacancies per unit volume, it is influenced by the excess vacancy concentration.

Mecking and Estrin [36] have developed a model that describes how the number of vacancies is influenced by plastic deformation. They estimated the number of vacancies produced mechanically in a unit volume per unit time as

$$P = 0.5\frac{\sigma\dot{\varepsilon}}{Gb^3} \tag{2.35}$$

The quantities in this equation have been explained above. The constant in Eq. (2.35) was estimated to 0.1 in [36]. A detailed derivation gives the value 0.5. For the excess vacancies the annihilation rate A was found to be

$$A = \frac{D_{\text{vac}}}{\lambda^2}(c - c_0) \tag{2.36}$$

where c_0 is the equilibrium vacancy concentration, $\Delta c = c - c_0$ the excess concentration, D_{vac} the diffusion constant for the vacancies, and λ the spacing between vacancy sinks. Following [36], λ can be related to the cell or subgrain size d_{sub}, Eq. (2.19) if a substructure is present. Combining Eqs. (2.19), (2.35) and (2.36), an expression for the excess vacancy concentration is obtained

$$\frac{\Delta c}{c_0} = 0.5\frac{\sqrt{2}K_{\text{sub}}^2\dot{\varepsilon}b^2}{D_{\text{self}}}\frac{G}{\sigma} \tag{2.37}$$

In finding Eq. (2.37), a relation for the self-diffusion coefficient has been applied

$$D_{\text{self}} = c_0\Omega D_{\text{vac}} \tag{2.38}$$

where Ω is the atomic volume. In the same way as in [36], the climb rate is assumed to be proportional to the total vacancy concentration. Equation (2.37) then gives the increase in the climb rate g_{climb} due to the presence of excess vacancy concentration

$$g_{\text{climb}} = 1 + \frac{\Delta c}{c_0} \tag{2.39}$$

The total climb mobility M_{climb} is obtained by multiplying Eq. (2.34) by g_{climb}.

$$M_{\text{climb}} = M_{\text{climb0}}g_{\text{climb}} \tag{2.40}$$

2.6.2 The Glide Mobility

The glide mobility is very high in a dislocation free crystal. A glide mobility of $M_0 = 1 \times 10^4$ 1/Pa/s was measured for a copper single crystal by Edington [37]. The mobility is much lower in an alloy where a forest of dislocations is present. As discussed above, jogs will be formed on the dislocations during deformation. Often the jogs will have to move perpendicular to their glide planes. This implies that they are sessile, and they have to move by climb [35], and this is a slow process. The motion of the jogs is likely to control the glide rate. This will be assumed and this is also what Hirth and Lothe did [35].

The starting point for the glide mobility is Eq. (2.40), since the jogs are moving by climb. However, there is another aspect that must be considered. Jogs are only present on a small part of a dislocation. Due to the slow movement of the jogs, the forces on the dislocations are localized to the jogs. The average distance between jogs can be related to the dislocation density ρ as $l_{\text{jog}} = 1/\sqrt{\rho}$. The Peach-Koehler formula $F = b\sigma l$ where l is the length of the dislocation gives the force F on a dislocation. F will be the force on each jog if l is chosen as l_{jog}. Thus, the stress on the jogs is raised by

$$g_{\text{glide}} = \frac{l_{\text{jog}}}{b} = \frac{1}{b\sqrt{\rho}} \tag{2.41}$$

where the length of a jog is set as the burgers vector. Equation (2.41) can be expressed in terms of the stress σ with the help of Taylor's equation

$$\sigma = \sigma_{\text{y}} + \alpha m_{\text{T}} G b \sqrt{\rho} \tag{2.42}$$

where σ_{y} is the yield strength

$$g_{\text{glide}} = \frac{\alpha m_{\text{T}} G}{\sigma - \sigma_{\text{y}}} \tag{2.43}$$

Multiplying the climb mobility by g_{glide} gives the glide mobility

$$M_{\text{glide}} = M_{\text{climb0}} g_{\text{climb}} g_{\text{glide}} \tag{2.44}$$

Equation (2.44) is applicable to both edge and screw dislocations. It is evident that the climb and glide mobility are closely related with the assumptions made. g_{glide} is approximately equal to the ratio between the shear modulus G and the applied stress σ. g_{glide} is always much larger than unity, since G is considerably larger than σ. As a consequence, the glide mobility is always larger than the climb mobility. When modeling creep, this is also a common starting point.

2.6.3 Cross-Slip Mobility

With the help of cross-slip, screw dislocations can change glide plane. This can increase the annihilation of dislocations with opposite Burgers vectors and raise the rate of recovery. There is an additional activation energy E_{cs} for cross-slip. Püschl gave the following values of E_{cs} [38].

$$E_{cs} = 0.012Gb^3 \frac{d_{SFE}}{b} \ln\left(\frac{2d_{SFE}}{b}\right) \tag{2.45}$$

d_{SFE} is the width of a stacking fault [35]

$$d_{SFE} = \frac{Gb^2}{8\pi\gamma_{SFE}} \frac{(2-\nu_P)}{(1-\nu_P)} \tag{2.46}$$

where γ_P is Poisson's ratio and γ_{SFE} the stacking fault energy. Taking copper and aluminum as examples with stacking fault energies of 45 mJ/m^2 and 166 mJ/m^2, respectively [39], Eq. (2.45) gives for E_{cs} values of 560 and 40 kJ/mol. This indicates strong temperature dependence for copper. Equation (2.45) is derived with the help of elasticity theory, which can give imprecise values at the atomic level. However, ab initio calculations have recently been carried out with similar results. Du et al. found E_{cs} values of 210 to 270 kJ/mol for Ni–Al alloys and Nöhring and Curtin 60 kJ/mol for Al–Mg, 160 kJ/mol for Cu–Ni and 180 kJ/mol for Ni–Al [40, 41]. Lower energy values have also been obtained in ab initio calculations. Rao et al. found values in the range 50–70 kJ/mol for Cu and Ni [42]. The effect of cross-slip on the mobility can be expressed as

$$g_{\text{cross-slip}} = \exp(-\frac{E_{cs}}{R_G T}) \tag{2.47}$$

$$M_{\text{cross-slip}} = M_{\text{climb0}} g_{\text{climb}} g_{\text{glide}} g_{\text{cross-slip}} \tag{2.48}$$

The role of cross-slip in dynamic recovery will be analyzed in Sect. 3.4.

2.6.4 The Climb Glide Mobility

The results for the dislocation mobilities are recent [8]. It has been known for a long time that the climb mobility in Eq. (2.34) underestimated the creep rates at low temperatures and high stresses by a wide margin. The main assumption was that glide would be the controlling mechanism under these conditions. To handle this situation a combined climb and glide mobility was formulated [43]

$$M_{\text{climb}} = M_{\text{climb0}} f_{\text{clglide}} \tag{2.49}$$

where f_{clglide} is given by

$$f_{\text{clglide}} = \exp\left(\frac{Q_{\text{self}}}{R_{\text{G}}T}\left(\frac{\sigma}{R_{\text{max}}}\right)^2\right) \tag{2.50}$$

R_{max} is the true tensile strength at ambient temperatures. It was work of Kocks et al. [44] that suggested the form of Eq. (2.50). They presented an empirical expression for the glide mobility. However, the expression had five unknown parameters and could therefore not be used directly. According to a suggestion by Nes, an integrated climb and glide mobility could be introduced [45]. In this way some of the unknown parameters could be found. With the aid of work by Chandler, the other parameters could be fixed [46].

The introduction of Eq. (2.50) has a number of important implications at low temperatures. First, the activation energy for creep is reduced. Second, the creep rate is increased by a large factor. Third, the stress exponent is raised in a dramatic way. These findings are in excellent accordance with experiments [15, 47].

Ideally, to describe creep, the basic models for the dislocation mobilities derived above should be used when modeling creep and other types of plastic deformation. However, since g_{climb} involves the strain rate, it is difficult to apply directly. Instead, the equations for the mobilities will be used to verify the validity of Eq. (2.50). This equation can then be applied to compute the creep rate. g_{climb} and f_{clglide} are compared in Figs. 2.5 and 2.6 for pure aluminum.

In Fig. 2.5, a continuous set of parameters for temperature and strain rate are used whereas in Fig. 2.6 experimental values are applied. It can be seen that the enhancement in vacancy concentration due to plastic deformation can fully explain the increase in creep rate in relation to the high temperature climb mobility. A second

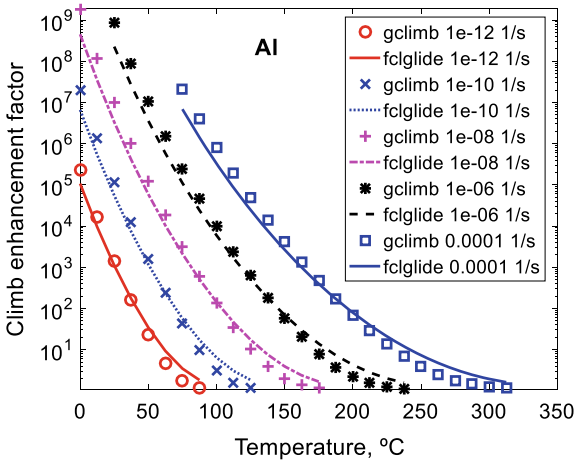

Fig. 2.5 Climb enhancement factor versus temperature at five strain rates for aluminum. The increase in vacancy concentration due to plastic deformation, Eq. (2.39) is compared to the climb-glide enhancement factor, Eq. (2.50). Redrawn from [8] with permission of intechopen

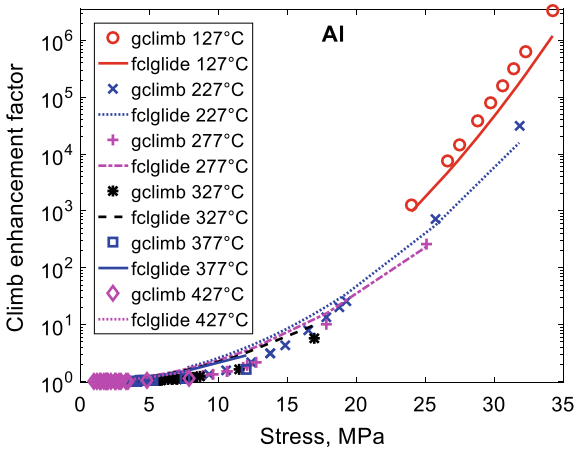

Fig. 2.6 Climb enhancement factor versus stress at six temperatures for aluminum. The increase in vacancy concentration due to plastic deformation, Eq. (2.39) is compared to the climb-glide enhancement factor, Eq. (2.50). Experimental data from [48]. Redrawn from [8] with permission of intechopen

example of the comparison is given in Figs. 2.7 and 2.8 for copper with 50 ppm P (Cu-OFP).

The two sets of models show an excellent agreement over many orders of magnitude of strain rate. The dependence of temperatures, stress and strain rate is well covered. It verifies that the expression for the climb-glide enhancement in Eq. (2.50) can be fully explained by the increase in vacancy concentration. Since its stress and temperature dependence is explicit, it is straightforward to apply. The total formula for the climb mobility, Eq. (2.49), with the equations for high temperature climb mobility M_{climb0}, Eq. (2.34), and the climb glide factor, Eq. (2.50) is now

$$M_{\text{climb}}(T,\sigma) = \frac{D_{\text{s0}}b}{k_{\text{B}}T} e^{\frac{\sigma b^3}{k_{\text{B}}T}} e^{-\frac{Q_{\text{self}}}{R_{\text{G}}T}} f_{\text{clglide}}(T,\sigma) \tag{2.51}$$

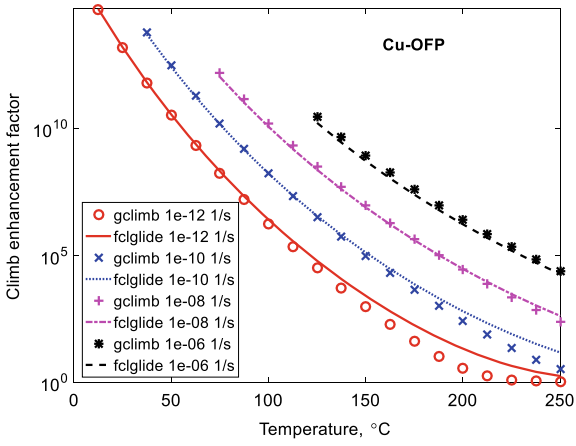

Fig. 2.7 Climb enhancement factor versus temperature at four strain rates for copper alloyed with 50 ppm P (Cu-OFP). The increase in vacancy concentration due to plastic deformation, Eq. (2.39) is compared to the climb-glide enhancement factor, Eq. (2.50)

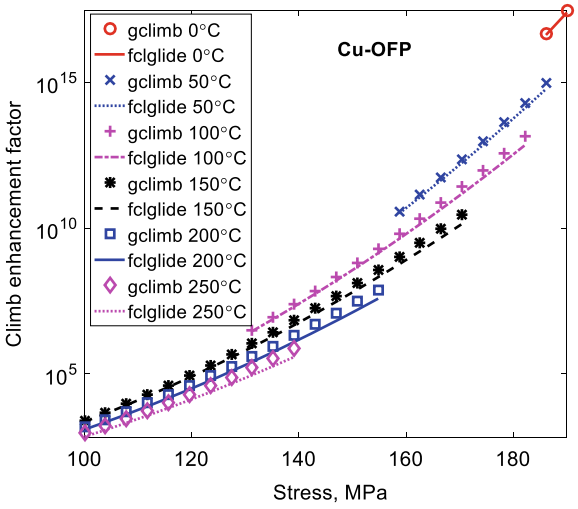

Fig. 2.8 Climb enhancement factor versus stress at six temperatures for copper alloyed with 50 ppm P (Cu-OFP). The increase in vacancy concentration due to plastic deformation, Eq. (2.39) is compared to the climb-glide enhancement factor, Eq. (2.50). Redrawn from [8] with permission of intechopen

This is the expression that should be inserted in the equation for the secondary creep rate (2.30)

$$\dot{\varepsilon}_{\text{sec}} = h_{\text{sec}}(\sigma - \sigma_i) \quad \text{where} \quad h_{\text{sec}}(\sigma) = \frac{2\tau_{\text{L}} b c_{\text{L}}}{m_{\text{T}}} M_{\text{climb}}(T, \sigma) \frac{\sigma^3}{(\alpha m_{\text{T}} G b)^3} \tag{2.52}$$

The derivation of the factor f_{clglide}, Eq. (2.50), was originally based on the assumption that it took the effect of glide into account. But the derivation now considers only climb. The result is that creep is fully climb controlled even at lower temperatures and higher stresses in the power-law breakdown regime.

2.7 Application to Aluminum

According to what we know today, static recovery is in general controlled by climb. This was analyzed in Sect. 2.3.3. This implies that Eq. (2.40) for the climb mobility should be applied in Eq. (2.30). Furthermore it was found that the enhancement factor for the climb mobility g_{climb} due to the increased vacancy concentration in Eq. (2.39) agreed with the climb glide enhancement factor f_{clglide} in Eq. (2.50). Further support to the use of Eq. (2.40) is found from the successful application of f_{clglide} to model experimental data.

An application of Eq. (2.30) will now be demonstrated for pure aluminum. In bcc metals dislocations are exposed to a friction stress, called the Peierls stress. The Peierls stress is usually not thought to be of significance for fcc alloys. However, it has recently been demonstrated by ab initio calculations that the Peierls stress is non-negligible for aluminum. A Peierls stress will be applied for σ_{i}. The following

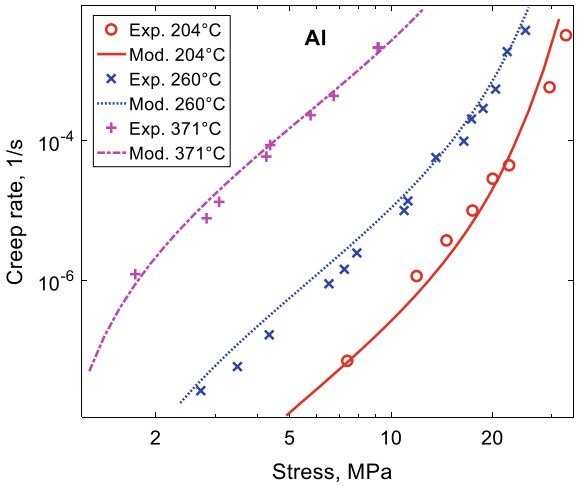

Fig. 2.9 Secondary creep rate versus stress for pure aluminum. Equation (2.30) is compared to experimental data from [50]. Reprinted from [8] with permission of intechopen

value for the Peierls stress of edge dislocations σ_{pe} was found by Shin and Carter [49].

$$\sigma_{\mathrm{pe}} = 4.9 \times 10^{-5} G \tag{2.53}$$

Screw dislocations gave much smaller values. The application of Eq. (2.30) is illustrated in Fig. 2.9.

The slope of the curves is about 4.5 at intermediate stresses in Fig. 2.9. The slope is the value of the stress exponent. The slope increases at higher stresses, indicating power-law breakdown. An increase of the stress exponent is also observed at low stresses. This is due to the presence of the Peierls stress. It can be seen that the model in Eq. (2.30) can obviously handle the experimental data quite well.

2.8 Application to Nickel

The factor f_{clglide} in Eq. (2.50) has been found to work with good precision for Al and Cu. It is used successfully in many places in this book for example also for austenitic stainless steels. It is an expression that is fitted to g_{climb} in Eqs. (2.37) and (2.39) and it may not be completely general. In fact, it has been found for nickel that a different expression has to be applied [51]. In this case, the starting point is to use the function for the secondary creep rate, Eq. (2.30) without the factor f_{clglide}.

$$\dot{\varepsilon}_{\mathrm{sec}} = 2\frac{bc_L\tau_{\mathrm{L}}}{m_{\mathrm{T}}} M_{\mathrm{climb0}}(T,\sigma) f_{\mathrm{SFE}} \frac{\sigma^3}{(\alpha m_{\mathrm{T}} G b)^3} \tag{2.54}$$

This formula for the creep rate is inserted into Eq. (2.37)

$$f_{\text{clglide}} = 1 + \frac{\Delta c}{c_0} = 1 + \frac{\sqrt{2} K_{\text{sub}}^2}{k_{\text{B}} T} \frac{b c_{\text{L}} \tau_{\text{L}}}{(\alpha m_{\text{T}})^3 m_{\text{T}}} f_{\text{SFE}} \frac{\sigma^2}{G^2} e^{\frac{\sigma b^3}{k_{\text{B}} T}} \tag{2.55}$$

For Ni, pipe diffusion, i.e. diffusion along dislocations is important. To the bulk diffusion coefficient in M_{climb0}, the pipe diffusion coefficient has to be added [29]

$$D_{\text{eff}} = D_{\text{self}} + \rho A_{\text{d}} D_{\text{d}} \tag{2.56}$$

where ρ is the dislocation density, A_{d} is the core area of the dislocations, and D_{d} the dislocation diffusion coefficient. For the core radius of the dislocations, a value of 6×10^{-10} m has been chosen. The values of the activation energy and pre-factor for the dislocation diffusion coefficient are 152.4 kJ/mol and 1.56×10^{-4} m^2/s [51, 52]. The creep rate can now be predicted using Eqs. (2.51), (2.52) and (2.55). Results are illustrated in Fig. 2.10.

There are important differences between Eqs. (2.50) and (2.55). At high stresses, Eq. (2.50) gives a stress exponent that increases with decreasing temperature that is a characteristic feature of creep in the power-law break down regime. On the other hand, Eq. (2.55) is associated with an essentially temperature independent stress exponent. In Fig. 2.10, the stress exponent is $n_{\text{N}} = 7$. Equation (2.54) in its basic form gives $n_{\text{N}} = 3$. Since pipe diffusion is dominant there is a contribution of 2 from the second term in Eq. (2.56), since ρ is proportional to the stress squared according to Taylor's Eq. (2.29). There is also a stress exponent contribution of 2 from Eq. (2.55). These contributions to the stress exponent add up to $n_{\text{N}} = 7$.

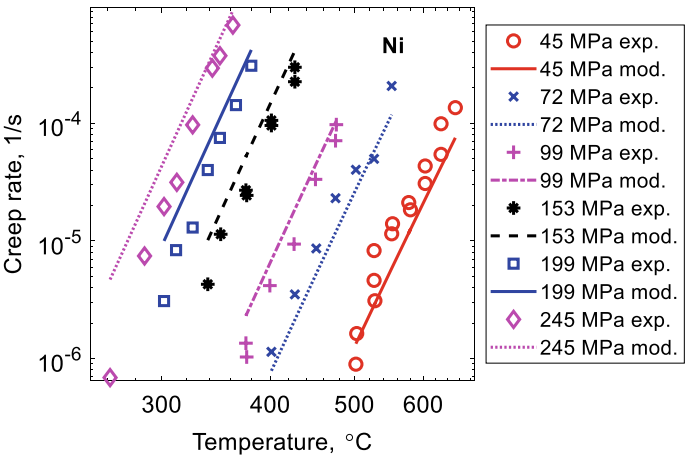

Fig. 2.10 Secondary creep rate versus temperature at six stresses for pure nickel. Predictions using Eqs. (2.51), (2.52) and (2.55) are compared to experimental data from [53]. Redrawn from [51] with permission of ASME

2.9 Summary

- In the past much creep research has been based on the Bird, Mukherjee and Dorn (BMD) equation. It describes the creep rate in the secondary stage as a function of temperature and stress. With the three to four adjustable parameters, most results for the creep rate can be described. It was for a long time assumed that the stress exponent and the activation energy would fall in a narrow range for specific creep mechanisms and that knowledge could be used to identify the operating mechanisms. However that assumption is challenged by more recent findings.
- The most important quantity in the modeling of creep is the dislocation density because it gives a large contribution to the creep strength. There are three main processes that control the development of the dislocation density: work hardening, dynamic recovery and static recovery. Models for the contribution from these three processes are derived. Differential equations for the time and strain derivative for the dislocation density are formulated. These equations are the starting point for much basic modeling of creep. From the equations, an expression for the secondary creep rate can be derived.
- Dislocation creep is assumed to be controlled by climb. The climb mobility is an important quantity in this respect. At low stresses the climb mobility is essentially stress independent and is only a function of the temperature. In this situation the models suggest a stress exponent of about three. During creep, strain induced vacancies appear. At higher stresses they have a dramatic effect on the stress exponent. Strain induced vacancies can quantitatively explain the high stress exponents at least up to 50 during power-law breakdown. This has been demonstrated for aluminum and copper.

References

1. F.H. Norton, *The creep of steel at high temperatures* (McGraw-Hill Book Co., New York, 1929)
2. J.E. Bird, A.K. Mukherjee, J.E. Dorn, Quantitative relation between properties and microstructure, in ed. by A.R.D.G. Brandon (Israel Universities Press, 1969), p. 255
3. O.D. Sherby, A.K. Miller, Combining phenomenology and physics in describing the high temperature mechanical behavior of crystalline solids. J. Eng. Mater. Technol. Trans. ASME **101**, 387–395 (1979)
4. F.C. Monkman, N.J. Grant, An empirical relationship between rupture life and minimum creep rate in creep-rupture tests. ASTM Proc. **1956**(56), 593–620 (1956)
5. J. Weertman, Steady-state creep through dislocation climb. J. Appl. Phys. **28**, 362–364 (1957)
6. J. Weertman, Steady-state creep of crystals. J. Appl. Phys. **28**, 1185–1189 (1957)
7. B. Wilshire, Observations, theories, and predictions of high-temperature creep behavior. Metall. Mater. Trans. A **33**, 241–248 (2002)
8. R. Sandström, Fundamental models for the creep of metals, in Creep, inTech (2017)
9. R. Lagneborg, Dislocation mechanisms in creep. Int. Metallur. Rev. **17**, 130–146 (1972)
10. U.F. Kocks, Laws for work-hardening and low-temperature creep. J. Eng. Mater. Technol. Trans. ASME, 98 Ser H, 76–85 (1976)

11. W. Roberts, Y. Bergström, The stress-strain behaviour of single crystals and polycrystals of face-centered cubic metals—A new dislocation treatment. Acta Metall. **21**, 457–469 (1973)
12. Y. Bergström, A dislocation model for the stress-strain behaviour of polycrystalline α-Fe with special emphasis on the variation of the densities of mobile and immobile dislocations. Mater. Sci. Eng. **5**, 193–200 (1970)
13. Y. Bergström, W. Roberts, A dislocation model for dynamical strain ageing of α-iron in the jerky-flow region. Acta Metall. **19**, 1243–1251 (1971)
14. F. Roters, D. Raabe, G. Gottstein, Work hardening in heterogeneous alloys—A microstructural approach based on three internal state variables. Acta Mater. **48**, 4181–4189 (2000)
15. R. Sandstrom, Basic model for primary and secondary creep in copper. Acta Mater. **60**, 314–322 (2012)
16. R. Wang, S. Wang, X. Wu, Edge dislocation core structures in FCC metals determined from ab initio calculations combined with the improved Peierls-Nabarro equation. Phys. Script. **83** (2011)
17. S. Mohamadnejad, A. Basti, R. Ansari, Analyses of dislocation effects on plastic deformation. Multiscale Sci. Eng. **2**, 69–89 (2020)
18. J. Friedel, *Dislocations* (Addison-Wesley, Reading (MA), USA, 1964)
19. R. Sandstrom, Subgrain growth occurring by boundary migration. Acta Metall. Mater. **25**, 905–911 (1977)
20. W. Blum, P. Eisenlohr, Dislocation mechanics of creep. Mater. Sci. Eng. A **510–511**, 7–13 (2009)
21. R. Sandström, The role of cell structure during creep of cold worked copper. Mater. Sci. Eng. A **674**, 318–327 (2016)
22. H. Magnusson, R. Sandstrom, Creep strain modeling of 9–12 pct Cr steels based on microstructure evolution. Metall. Mater. Trans. A **38A**, 2033–2039 (2007)
23. D. Francke, W. Pantleon, P. Klimanek, Modelling the occurrence of disorientations in dislocation structures. Comp. Mater. Sci. **5**, 111–125 (1996)
24. P. Ambrosi, C. Schwink, Slip line length of copper single crystals oriented along [100] and [111]. Scr. Metall. **12**, 303–308 (1978)
25. M.R. Staker, D.L. Holt, The dislocation cell size and dislocation density in copper deformed at temperatures between 25 and 700 °C. Acta Metall. **20**, 569–579 (1972)
26. H. Wiedersich, Hardening mechanisms and the theory of deformation. JOM **16**, 425–430 (1964)
27. W. Blum, P. Eisenlohr, F. Breutinger, Understanding creep—A review. Metall. Mater. Trans. A **33**, 291–303 (2002)
28. S. Vujic, R. Sandstrom, C. Sommitsch, Precipitation evolution and creep strength modelling of 25Cr20NiNbN austenitic steel. Mater. High Temp. **32**, 607–618 (2015)
29. O.A. Ruano, A.K. Miller, O.D. Sherby, Influence of pipe diffusion on the creep of fine-grained materials. Mater. Sci. Eng. **51**, 9–16 (1981)
30. H. Magnusson, R. Sandstrom, The role of dislocation climb across particles at creep conditions in 9 to 12 pct Cr steels. Metall. Mater. Trans. A **38A**, 2428–2434 (2007)
31. P. Ostrom, R. Lagneborg, Recovery-athermal glide creep model. J. Eng. Mater. Technol. Trans. ASME 98 Ser H, 114–124 (1976)
32. A.H. Delandar, R. Sandström, P. Korzhavyi, The role of glide during creep of copper at low temperatures. Metals **8** (2018)
33. M. Biberger, J.C. Gibeling, Analysis of creep transients in pure metals following stress changes. Acta Metall. Mater. **43**, 3247–3260 (1995)
34. B. Wilshire, M. Willis, Mechanisms of strain accumulation and damage development during creep of prestrained 316 stainless steels. Metall. Mater. Trans. A: Phys. Metallur. Mater. Sci. **35 A**, 563–571 (2004)
35. J.P. Hirth, J. Lothe, *Theory of dislocations* (Krieger, Malabar, Florida, 1982)
36. H. Mecking, Y. Estrin, The effect of vacancy generation on plastic deformation. Scr. Metall. **14**, 815–819 (1980)
37. J.W. Edington, The influence of strain rate on the mechanical properties and dislocation substructure in deformed copper single crystals. Phil. Mag. **19**, 1189–1206 (1969)

38. W. Püschl, Models for dislocation cross-slip in close-packed crystal structures: a critical review. Prog. Mater. Sci. **47**, 415–461 (2002)
39. X.-Z. Wu, R. Wang, S.-F. Wang, Q.-Y. Wei, Ab initio calculations of generalized-stacking-fault energy surfaces and surface energies for FCC metals. Appl. Surf. Sci. **256**, 6345–6349 (2010)
40. J.-P. Du, C.-Y. Wang, T. Yu, Cross-slip process in model Ni(Al) solid solution: an embedded-atom method study. Comp. Mater. Sci. **91**, 192–199 (2014)
41. W.G. Nöhring, W.A. Curtin, Dislocation cross-slip in fcc solid solution alloys. Acta Mater. **128**, 135–148 (2017)
42. S.I. Rao, D.M. Dimiduk, T.A. Parthasarathy, J. El-Awady, C. Woodward, M.D. Uchic, Calculations of intersection cross-slip activation energies in fcc metals using nudged elastic band method. Acta Mater. **59**, 7135–7144 (2011)
43. R. Sandstrom, H.C.M. Andersson, Creep in phosphorus alloyed copper during power-law breakdown. J. Nucl. Mater. **372**, 76–88 (2008)
44. U.F. Kocks, Argon A.S., Ashby, M.F., Thermodynamics and kinetics of slip. Prog. Mater. Sci. **19**, 1 (1975)
45. E. Nes, K. Marthinsen, Modeling the evolution in microstructure and properties during plastic deformation of f.c.c.-metals and alloys—An approach towards a unified model. Mater. Sci. Eng.: A **322**, 176–193 (2002)
46. H.D. Chandler, Effect of unloading time on interrupted creep in copper. Acta Metall. Mater. **42**, 2083–2087 (1994)
47. R. Sandström, Fundamental models for creep properties of steels and copper. Trans. Indian Inst. Met. **69**, 197–202 (2016)
48. H. Mecking, A. Styczynski, Y. Estrin, *Steady state and transient plastic flow of aluminium and aluminium alloys, in strength of metals and alloys (ICSMA 8)* (Pergamon, Oxford, 1989), pp.989–994
49. I. Shin, E.A. Carter, Possible origin of the discrepancy in Peierls stresses of fcc metals: first-principles simulations of dislocation mobility in aluminum. Phys. Rev. B—Condensed Matter Mater. Phys. **88** (2013).
50. I.S. Servi, N.J. Grant, Creep and stress rupture behaviour of aluminium as a function of purity. Trans. AIME **191**, 909–916 (1951)
51. R. Sandström, J. Zhang, Modeling the creep of nickel. J. Eng. Mater. Technol. **143** (2021)
52. S. Soltani, N. Abdolrahim, P. Sepehrband, Mechanism of intrinsic diffusion in the core of screw dislocations in FCC metals—A molecular dynamics study. Comp. Mater. Sci. **144**, 50–55 (2018)
53. E.C. Norman, S.A. Duran, Steady-state creep of pure polycrystalline nickel from 0.3 to 0.55 Tm. Acta Metall. **18**, 723–731 (1970)